Percolating Metallic Structures Templated on Laser-deposited Carbon Nanofoams derived from Graphene Oxide: Applications in Humidity Sensing

Sebastian Nufer[a,b], Dimitrios Fantanas[a,c], Sean P. Ogilvie[b], Matthew J. Large[b], Dominik J. Winterauer[d,e], Jonathan P. Salvage[f], Manuela Meloni[b], Alice A. K. King[b], Pascale Schellenberger[b], Aleksey Shmeliov[g], Sandra Victor-Roman[h], Mario Pelaez-Fernandez[i], Ana Benito[h], Valeria Nicolosi [g], Raul Arenal [i,j], Wolfgang Maser[h], Adam Brunton [a], Alan B. Dalton[b*]*

a M-Solv Ltd, Oxonian Park, Langford Locks, Kidlington, Oxford, OX5 1FP, UK
b University of Sussex, Department of Physics and Astronomy, Brighton, BN1 9RH, UK
c University of Surrey, Department of Physics, Guildford, GU2 7XH, UK
d Renishaw, New Mills, Wotton-under-Edge, Gloucestershire, GL12 8JR, UK
e Institute des Matériaux Jean Rouxel (IMN), Physics of Materials and Nanostructures, Nantes, 44322, France
f University of Brighton, School of Pharmacy and Biomolecular Science, Brighton, BN2 4GJ, UK
g Trinity College Dublin, School of Chemistry and CRANN, Dublin 2, Ireland
h Instituto de Carboquimica, CSIC, Zaragoza, E-50015, Spain
i Instituto de Nanociencia de Aragón, Universidad de Zaragoza, Laboratorio de Microscopias Avanzadas (LMA),50018 Zaragoza, Spain
j Fundacion ARAID, 50018 Zaragoza, Spain

KEYWORDS: carbon nanofoam, reduced graphene oxide, humidity sensor, scaffold, specificity, selectivity

Abstract

Carbon nanofoam (CNF) is a low-density, high-surface-area material formed by aggregation of amorphous carbon nanoparticles into porous nanostructures. We report the use of a pulsed infrared laser to prepare CNF from a graphene oxide (GO) target material. Electron microscopy shows that the films consist of dendritic strings which form web-like three-dimensional structures. The conductivity of these structures can be modified by using the CNF as a nanostructured scaffold for gold nanoparticles deposited by sputter coating, controllably increasing the conductivity by up to four orders of magnitude. The ability to measure the conductivity of the porous structures allows electrochemical measurements in the environment. Upon decreasing humidity, the pristine CNF exhibits an increase in resistance with a quick response and recovery time. By contrast, the gold-sputtered CNF showed a decrease in resistance, indicating modification of the doping mechanism due to water adsorption. The sensitivity to humidity is eliminated at the percolation threshold of the metal on the CNF.

1. Introduction

It is well understood that laser irradiation can be used to achieve the selective thermal reduction of graphene oxide.[1] The literature discusses the use of numerous laser types and processes to achieve films of reduced graphene oxide (rGO) with sheet resistance as low as 50 Ω per square.[1–4] Since this method is inherently selective it can be used to produce patterned structures;[5] such as

transistors[3,6], supercapacitor electrode geometries[7] and sensor devices.[8] The range of laser fluences used to reduce the GO are typically between 20 mJ/cm^2 to 400 mJ/cm^2. In a small window of fluences carbon foam is created as a by-product of the reduction process.

Carbon foam is a low-density, porous form of amorphous nanostructured carbon which can be produced in various morphologies and with different methods.[9] The fundamental formation mechanism is described by Henley et al.[10] Nanoscale carbon clusters are formed through three processes during the GO reduction: condensation of carbon atoms within the plume of material vaporized by the laser; direct ablation of clusters of the target material, and the subsequent aggregation of smaller clusters. These carbon clusters then grow by the attachment of single carbon atoms. The formation occurs outside of the initial shock wave created by the laser when ablating the target, where the carbon starts to diffuse. Deposition within the shock wave would lead to a dense graphitic film. The individual clusters are formed of between 15% and 45% of sp^3 carbon, with the sp^3 bonding prevalent at the cluster surface; this surface structure is responsible for the bonding between individual clusters.[11] At the nanoscale the assembled clusters form a fractal morphology, with the microscale structure having a web-like appearance.

Rode et al.[11] described the formation of a fractal carbon foam, during the laser ablation of a carbon target, with similar properties to Schwarzites. Rode et al. subsequently coined the phrase “carbon nanofoam” (CNF) to describe this type of material.[12] Munoz et al.[13] reported clustered carbon foam formation during ablation of an organometallic gold salt in air under ambient conditions, which led to the production of a nanocomposite with gold particles enclosed within the carbon clusters. Zani et al.[14] investigated pulsed laser deposition of carbon foam onto silicon achieving a uniform film across 1 μm^2. Spanakis et al.[15] investigated the use of CNF for preparation of supercapacitor

electrodes. They sputtered 2 nm thick gold layers on to the CNF electrodes to enhance their specific capacitance up to 130 Fg^{-1}.

The high specific surface area of the CNF makes it an ideal material for sensing applications. The conductivity of carbon materials in sensing applications is strongly influenced by changes in humidity.[16–20] Especially in gas sensing applications humidity results in cross-talk and reduces selectivity of the materials. In order to enhance selectivity the influence of humidity on the materials' response needs to be reduced. One well known method for achieving this is the use of metal functionalisation.[21,22]

In the present work, we investigate the conductivity response of pristine CNF and materials decorated with gold nanoparticles when exposed to changes in humidity. The CNF was deposited using a pulsed infrared laser and a GO target. Upon decreasing the humidity the conductivity of the pristine CNF decreases due to desorption of water ions from the surface. By contrast, the conductivity of the gold-coated CNF increases when the humidity decreases due to the reduction of depletion regions induced by the adsorbed water on the gold coating. At the percolation threshold of the metallic coating the two counteracting sensing mechanisms appear to cancel each other out, making the CNF insensitive to changes in humidity. This first presentation of CNF for sensing application shows how tuned functionalisation can eliminate cross-talk of humidity in a sensing device.

2. Results and Discussion

Atomic force microscopy (AFM) in Figure 1a of the as-received GO material reveals a flake size between 500 nm and 1 μm and a uniform flake thickness of 2 nm. The Raman spectra of the GO

after initial heat treatment and the rGO after laser treatment are shown in Figure 1b. Figure 1c and 1d show the window of laser fluence where CNF is formed during the reduction of the GO. In Figure 1c the GO is heat treated to various temperatures, whereas in Figure 1d the thickness of the deposited GO film before reduction is changed and then heat treated to 250 °C. The window of fluence where CNF formation is observed appears to be invariant under these different experimental conditions. CNF is only formed in a window of fluences, independent of the substrate processing. The sheet resistance of the rGO is not influenced by the production of the CNF. At low fluences the laser shows no interaction with the GO. At fluences above the CNF production window the ablation threshold of the GO is overcome and clear laser ablated trenches are produced. The process of depositing the CNF onto a substrate with interdigitated electrodes (IDE) is illustrated schematically in Figure 2. Laser ablated electrodes on glass are separated by an uncoated region so the laser is able to shine through the transparent substrate (Figure 2Ai). The GO is transformed into CNF from the interaction with the laser (Figure 2Aii) and is deposited onto the electrodes. By scanning the laser up and down the entire electrode areas are covered with CNF (Figure 2Aiii). Figure 2Aiv shows the electron micrograph of material deposited on pre-patterned

electrodes. Figure 2Bi illustrates the functionalization process through sputtering and a structure of the functionalized material is presented in Figure 2Bii.

The deposited CNF shows a web-like appearance as seen in the SEM image in Figure 3a. A transmission electron microscopy (TEM) image, shown in Figure 3b, shows the dendritic strings which comprise the web-like structure seen at lower magnification.

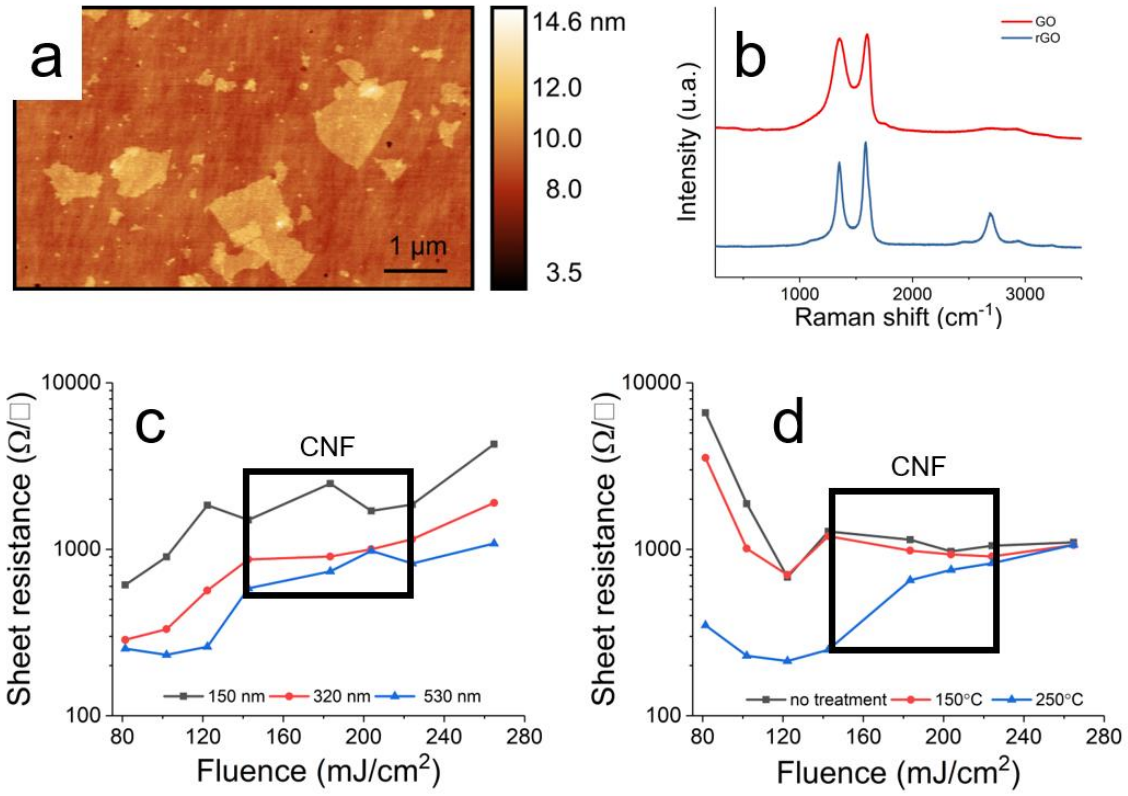

Figure 1 a) AFM image of synthesized GO, b) Raman spectra of heat treated GO and laser reduced GO, c) Sheet resistance of rGO for various fluences where the thickness of the GO was changed, inset window shows where CNF occurring, d) Sheet resistance of rGO for various fluences where the temperature treatment of the GO is changed, inset window shows where CNF occurring

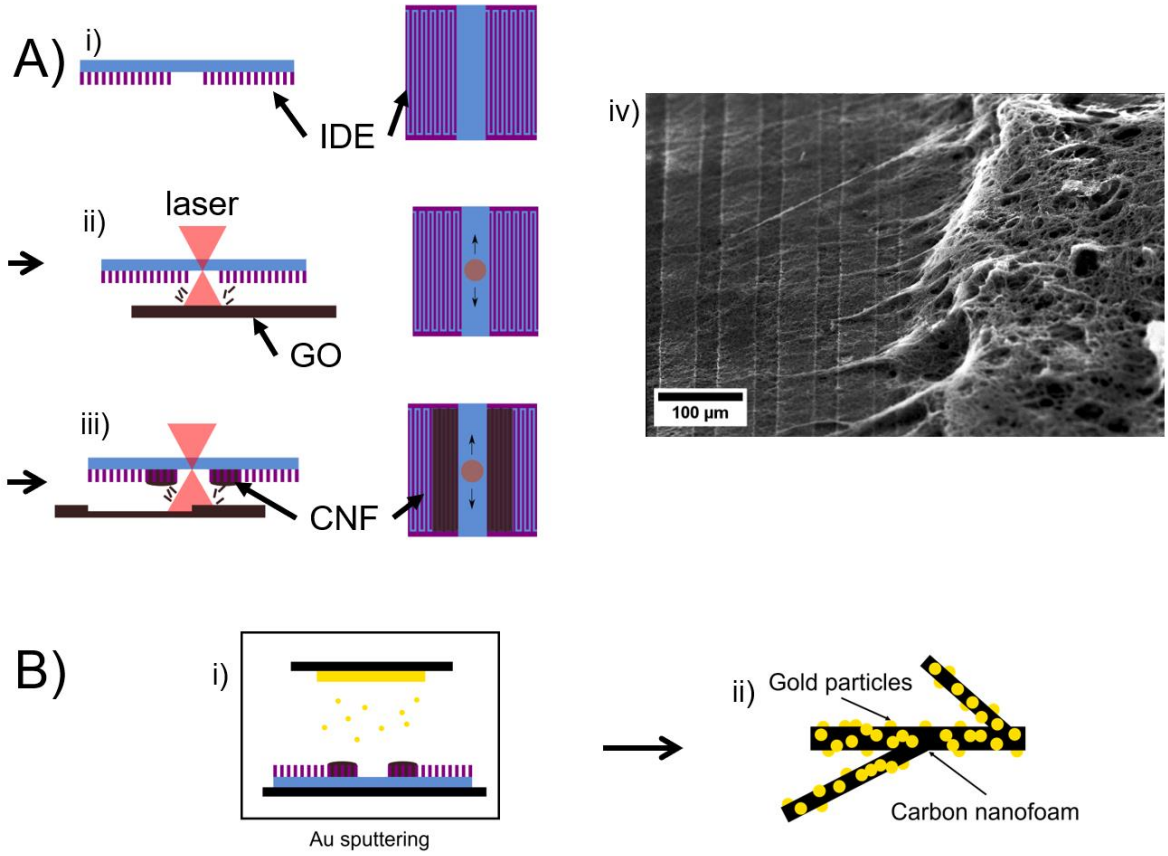

Figure 2: Ai) Schematic of laser ablated electrodes on glass substrate where the electrodes are separated in two parts so the laser can go through the glass to ablate the GO target beneath (Aii) to transform the GO into CNF, by moving the laser along the electrodes CNF is deposited over the entire length of the electrodes (Aiii), Aiv) shows an SEM images of the CNF on IDEs, Bi) shows the functionalization process through sputtering, Bii) shows the schematic of the functionalized CNF with Au particles.

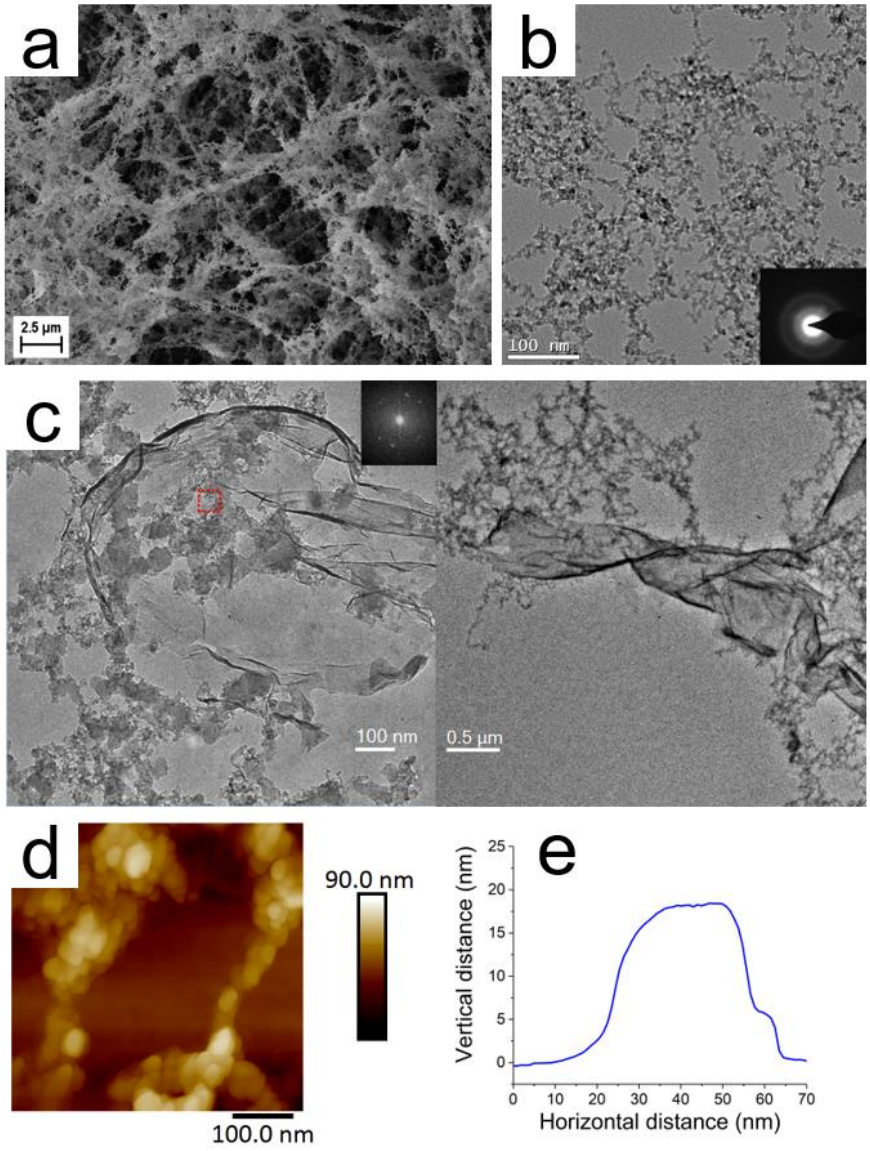

Figure 3 a) SEM image of uncoated CNF made from GO, b) TEM image of the CNF, a fractal analysis yields a fractal dimension of 1.6, the inset shows the transmission electron diffraction pattern showing the structure is amorphous, c) TEM images acquired at low temperatures of rGO flake transferred into the CNF, inset FFT shows crystalline structure of overlapping rGO flakes d) AFM picture of a string of the uncoated CNF structure, e) height analysis of insets in AFM image, the measured thickness is 18 nm

Using a low magnification TEM image (supplementary information Figure S1) a fractal dimension of 1.6 is measured, which shows that the strings are dominant in the formation of the overall network.

The TEM images acquired at low temperature in Figure 3c show that during the laser processing the GO is not completely transformed into CNF but individual flakes are transferred from the target to the substrate. The GO flakes are reduced into rGO during the transfer, and these rGO flakes are sparsely distributed through the CNF film. During laser ablation it is common for some parts of the material to redeposit on the laser target.[23] In the case of reducing graphene oxide not only re-deposition occurs but also a deoxygenation as locally high temperatures are induced, in a so-called laser shock hardening process.[1,24] The oxygen release in the material induces a pressure build up which can lead to exfoliation of the material being illuminated.[4,25] This leads us to believe the sheets of rGO in the CNF are a result of a combined process of re-deposition during the reduction of the graphene oxide and the laser induced exfoliation. The distribution of these rGO sheets is so sparse that they are not expected to greatly influence the conductivity of the CNF film.

The AFM micrograph of a foam sample in Figure 3d shows the cluster assembly of strings, as seen in the TEM. The dimensions are in the nanometre regime; approximately 18 nm for the region shown in Figure 3e. The broad, overlapping D and G modes in the Raman analysis (Figure S2) of the foam are indicative of amorphous carbon materials.[26] The dendritic growth seen in the TEM images, the cluster formation visible in the AFM image and the web-like structure over greater length scales in the SEM image is consistent with the explanations of CNF growth by Rode et al.[11,12] and Henley et al.[10]

The structure and conductivity of the CNF can be modified by sputter coating with gold as shown in Figure 4a. While film thickness is poorly-defined for such porous structures, thickness measurements were performed with the focus drive of an optical microscope and an averaged value (film thickness of 100 µm) was used for conductivity calculations. The conductivity as a function of sputtering time is shown in Figure 4b.

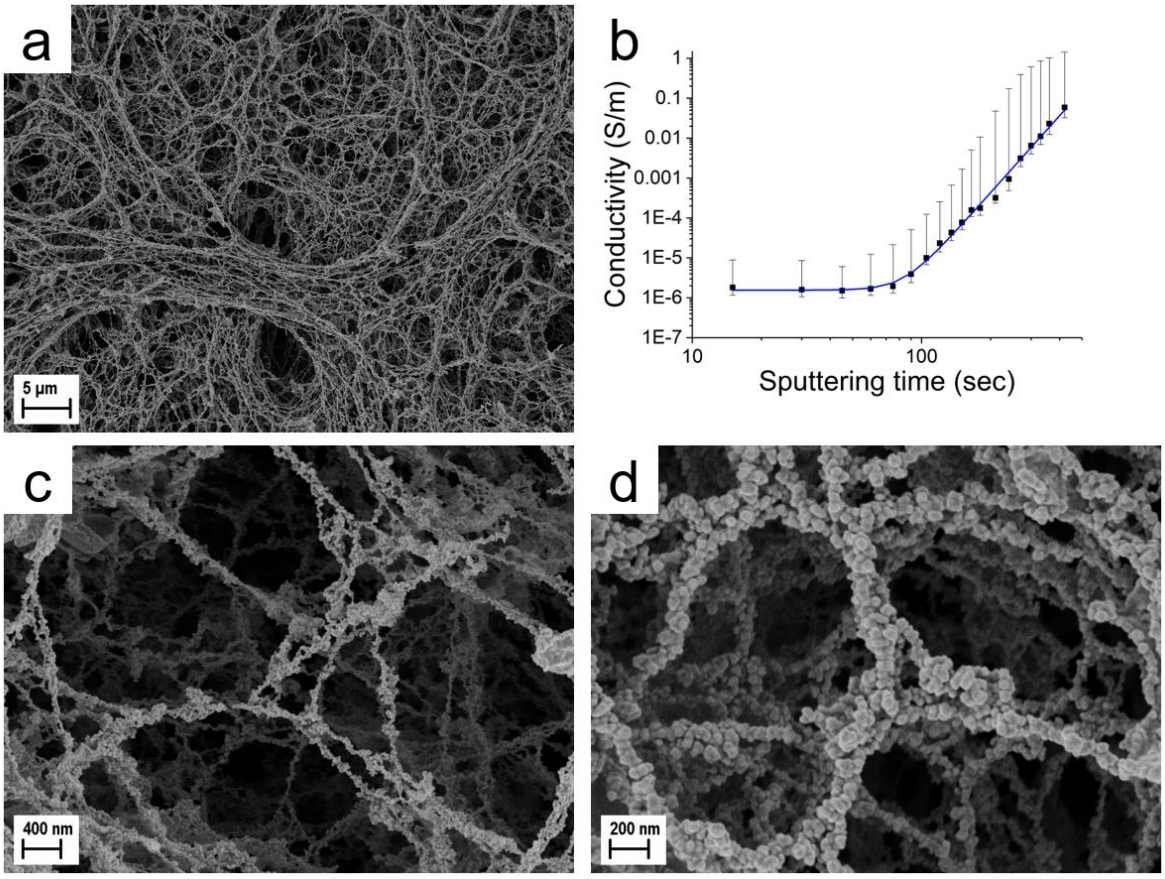

Figure 4 a) Low magnification SEM of a metal-coated CNF film. b) Conductivity values over different sputtering times with percolation fitting performed; SEM of CNF film after (c) 2 min , (d) 5 min of sputtering.

The initial conductivity of the unmodified CNF material was 3 μS/m; upon coating with gold this increased to 58 mS/m after 7 min sputtering time. We can clearly see multiple regimes in the conductivity data of Figure 4b. Below 60 s sputtering time the CNF conductivity does not significantly vary. SEM images of the deposited material at 15 s (Figure S3a) and at 45 s (Figure S3b) show that the CNF maintains its "fluffy" structure, albeit sparsely decorated with gold nanoparticles. Around 60 to 70 s we observe that the conductivity begins to increase, with the data beyond that point resembling a power law dependence. This behaviour is characteristic of a percolating system, with the parameter space (sputtering time) separated into below and above percolation regimes. [27] Figure 4c and 4d show the increase of gold coating on the CNF strings forming a metallic network. Once the density of gold on the CNF surpasses the percolation threshold the gold coating on the CNF begins to dominate the conductivity. The data of Figure 4b are fitted using a percolation scaling of the form $\sigma = A(t - t_c)^n + \sigma_0$; where σ is the conductivity; A is a pre-factor; t is the sputtering time; t_c is the percolation threshold; n is the conductivity exponent; σ_0 is the baseline CNF conductivity. We find the percolation threshold sputtering time to be 1 min, equivalent to a 3 nm thick gold layer on a flat surface. The increase in conductivity after the percolation threshold is smeared out due to the porous structure of the CNF. The power law curve would eventually saturate when all the pores are filled with gold.

The CNF inherently has a very high surface area that can be utilised in applications such as sensors or supercapacitors. Figure 5a shows the initial conductivity and response of the CNF to a change in humidity from 37 %rh to 20 %rh at different sputtering times. Figure 5b shows the time response of the uncoated pristine CNF. We note that below the percolation threshold the sample resistance increases with decreasing humidity, with a rapid recovery to the initial state once the initial humidity is restored. Treating the signal as a rising followed by a decaying exponential, we find

time constants (t_{90}, the time required to achieve 90% of the limiting response) of 13 s for the water desorption and <1 s for the subsequent water reabsorption. Above the percolation threshold the opposite effect is observed, with water desorption and adsorption occurring over significantly longer timescales; 32 s and 65 s for the desorption and recovery, respectively. Very close to the percolation threshold, the two apparently competing behaviours 'cancel out' to give an extremely low response to the humidity change. Figure 5c shows an analogous measurement to Figure 5b close to the gold percolation threshold, and Figure 5d shows the response within the percolating regime.

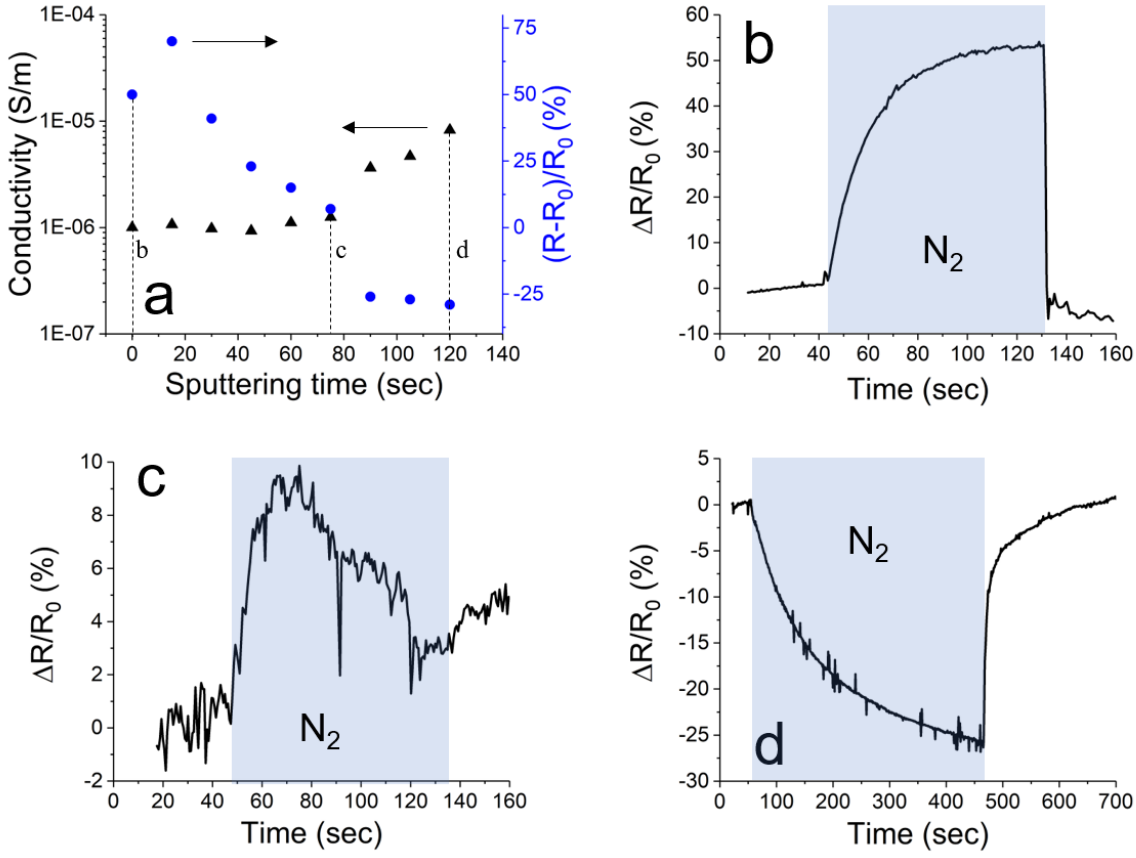

Figure 5 (a) Influence of sputtering time to response of sensor and conductivity to relative humidity change of 17 %, (b) Sensor response to a relative humidity change of 17% of uncoated sample, (c) Sensor response a relative humidity change of 17% when sputtered for 75 sec, (d) Sensor response a relative humidity change of 17% when sputtered for 120 sec

The above measurements show how the network changes its sensing behaviour from a carbon response to a metallic response. A decrease in humidity leads to a decrease in conductivity in the amorphous carbon network as the water layer on the carbon becomes discontinuous and slows down the H_2O-H_3O^+ transfer. This ionic transfer is the main water sensing mechanism in carbon-based systems.[28] By contrast, in the Au/CNF network where the conductivity is dominated by the gold, the adsorbed water induces depletion zones in the gold where it is attached. Removing water from the surface of the gold by reducing the humidity reduces the influence of the depletion zones so the conductivity increases.[29]

A gold film sputtered directly onto electrodes (without the supporting CNF) with a similar resistance as the gold and carbon nanofoam hybrid (Au/CNF) of Figure 5d results in a response of only 7 % in the same experimental conditions. This effect can be attributed to the increased surface area available for the water to interact with the gold in the Au/CNF network and the increased influence of the depletion zones due to the nanometric size of the percolating gold particles.

The response of the sensors prepared to the humidity change in our experiments is high, with a maximum response of 70 % to a change of 18 %rh in the CNF sensor and a response of 30 % in the Au/CNF sensor. The response time of the CNF network is quicker than for the Au/CNF film but both have an excellent recovery time. While we expect that precisely at the percolation threshold the system itself should not be sensitive to a change in humidity, the competing effects of both the carbon response and the gold response can be seen in the device near percolation in Figure 5c. Lastly, we evaluate the sensitivity S of our devices, which is defined as

$$\boldsymbol{S} = \frac{\frac{\boldsymbol{R} - \boldsymbol{R_0}}{\boldsymbol{R_0}} \times 100}{\Delta\%\boldsymbol{rh}}$$

where R is the measured resistance, R_0 is the baseline resistance, Δ%rh is the change in humidity during the exposure.[30] For the CNF and Au/CNF hybrids respectively we find values of 3.89 and 1.70. For this limited range of measured humidity this sensitivity can compete with or exceed existing carbon-based humidity sensors based on a chemiresistor with DC bias.[16–18,30]

3. Conclusion

Carbon nanofoam has been formed as a by-product of the laser reduction of a GO precursor using an infrared pulsed laser. CNF appears only in a small window of fluences during the reduction process. Characterization of the CNF showed dendritic cluster assembly of carbon into fine structures with nanometre sized features. The CNF acts as nanostructured scaffold for sputtered gold. The metallization of the carbon structure results in a different surface doping mechanism compared to the pristine foam. Whereas the uncoated CNF is dominated by the transfer of electrons from the water ion transformation, the metallic structure is dominated by water induced depletion zones within the metal. These two mechanisms lead to opposing conductivity responses in the Au/CNF network. At percolation the two mechanisms counteract each other leading to a suppression of the sensitivity to a change in humidity. The tunability of the conductivity together with the high surface area may enable applications such as supercapacitors or gas sensors with diminished sensitivity to environmental water. The response of the CNF towards a change in humidity can compete with, or exceed, the performance of current sensors based on the same principle. This sensor design allows for increased selectivity by eliminating cross-talk due to humidity.

4. Experimental

Graphite oxide was prepared from graphite powder (Sigma Aldrich, Ref. 332461) using a modified Hummers' method as described elsewhere. [31,32] In brief, 170 mL of concentrated H_2SO_4 was added to a mixture of graphite flakes (5.0 g) and $NaNO_3$ (3.75 g). The mixture was vigorously stirred for 30 minutes in an ice bath. $KMnO_4$ (25 mg) was slowly added while stirring for another 30 minutes. The reaction was then warmed up to 35 ºC and stirred overnight. Subsequently, distilled water (250 ml) and 30% H_20_2 (20 mL) were slowly added in sequence. The mixture was stirred for 1 hour, filtered and washed repeatedly with 400 mL of HCl:H_2O (1:10), and dried in air, thus yielding graphite oxide. Finally, the resulting graphite oxide was dispersed in water at a concentration of 2 mg/mL and bath sonicated for 2 hours. This led to a brown-colored dispersion of exfoliated graphene oxide flakes.

The GO dispersion was spray deposited on to untreated soda-lime glass substrates using a hand-held air brush (Badger Model XL2000). The glass substrate was placed on a hotplate to enhance the evaporation rate of the water. Multiple spray passes were used to deposit a film with a thickness approximately 200 nm. The sample was then placed in an oven and the temperature was ramped to 250°C over 1.5 hours and then taken out cool at room temperature.

An MSV-101 (M-Solv Ltd, Oxford) laser materials processing machine, equipped with a 1064 nm wavelength, nanosecond-pulsed laser (Multiwave MOPA-DY Series Pulsed Fiber Laser, set to 10 ns pulse duration and 200 kHz pulse repetition frequency) and galvoscanner was used for the GO reduction and consequent deposition of the CNF. For the CNF fluence window determination a frequency of 100 kHz and a mark speed of 30 mm/sec was used. For the deposition a glass substrate

with molybdenum on top laser ablated into IDEs was placed 1 mm above the GO target. The laser beam was set up to pass through the (transparent) slide and its 25 μm focal spot was scanned over the GO partly reducing it to reduced GO and partly ablating it which results in the deposition of CNF on to the glass. The slide was kept stationary while the GO target was moved in by 7 μm, orthogonal to the laser scan direction, after each pass of the beam, to expose fresh GO target material. The laser fluence was set to 400 mJ/cm^2 with a scan speed of 100 mm/s.

Samples were imaged with a Zeiss SIGMA field emission gun scanning electron microscope (FEG-SEM) using a Zeiss in-lens secondary electron detector. The FEG-SEM working conditions used were; 2.5 kV accelerating voltage, 20 μm aperture, and 2 mm working distance. A Bruker Dimension Icon atomic force microscope (AFM) was used in peak force mode to measure topography.

The Raman measurements were carried out with a Renishaw inVia confocal Raman microscope with a 532 nm solid-state laser and a x50 objective lens (NA=0.75). GO and reduced GO were probed with 0.6 mW and the CNF with 0.06 mW laser intensity.

Gold was sputtered using a BIO-RAD SC 510 'cool' sputter coater. The current was held constant at 20 mA, the chamber vacuum was held at a constant pressure of 0.1 mbar. The thickness was controlled by varying the sputtering time.

Humidity measurements were performed using pressurized nitrogen and a Alicat mass flow controller to maintain a flowrate of 500 sccm. The CNF was placed in a small measurement chamber (200 ml volume) contacted to measure its resistance using a Keithley 2420 source meter by applying a constant current and monitoring the voltage across the device. The baseline was measured at ambient with an open lid, the lid was closed and the chamber purged with nitrogen

while the resistance was monitored. When the signal reached steady state the flow of nitrogen was interrupted and the lid opened to expose the device to ambient again. The humidity changed from 38 %rh at ambient to 20 %rh in the nitrogen environment.

The CNF was deposited onto a on the substrate mounted holey carbon grid. The shape of the nanofoam was imaged using a transmission electron microscope (TEM) FEI Titan operating at 300 keV. Both bright field TEM and annular dark field scanning TEM modes were used. HRTEM images were taken at a FEI Titan High-Base microscope equipped with a CEOS CETCOR Cs objective lens corrector, working at 80 keV and a low temperature. Images were acquired using a Gatan 626 single-tilt liquid nitrogen cryo-holder, allowing for the sample to be kept at ~77 K while performing this study.

ASSOCIATED CONTENT

Supporting Information

The Supporting Information is available free of charge on the ACS Publications website at DOI:

Low magnification TEM image, Raman spectrum, more SEM images

AUTHOR INFORMATION

Corresponding Author

***E-mail: sebastian.nufer@m-solv.com**

***E-mail: A.B.Dalton@sussex.ac.uk**

Funding Sources

Marie Sklodowska-Curie grant agreement No 642742, Graphene Flagship grant agreement 696656, the Spanish Ministerio de Economia y Competitividad (MAT2016-79776-P, (AEI/FEDER, UE)), Construyendo Europa desde Aragon 2014-2020 (grant number E/26), MINECO and AEI (project ENE2016-79282-C5-1-R and associated EU Regional Development Funds), Gobierno de Aragón (Consolidated Group DGA-T66-GCNN and associated EU Social Funds), MINECO (BES2014-068727 and associated EU Social Funds)

ACKNOWLEDGMENT

Graham Booth's work is highly appreciated helping to set up the deposition system. This work has received funding from the European Union's Horizon 2020 research and innovation program under the Marie Sklodowska-Curie grant agreement No 642742 as well as for EU H2020 program "Graphene Flagship" (Grant Agreement 696656). R.A. gratefully acknowledges the support from the Spanish Ministerio de Economia y Competitividad (MAT2016-79776-P, (AEI/FEDER, UE)), from the Government of Aragon and the European Social Fund under the project "Construyendo Europa desde Aragon" 2014-2020 (grant number E/26). A.M.B and W.K.M gratefully acknowledge the financial support from Spanish MINECO and AEI (project ENE2016-79282-C5-1-R and associated EU Regional Development Funds), and the Gobierno de Aragón (Consolidated

Group DGA-T66-GCNN and associated EU Social Funds). SVR thanks Spanish MINECO for her PhD grant (BES2014-068727 and associated EU Social Funds).

ABBREVIATIONS

AFM atomic force microscope, CNF carbon nanofoam, GO graphene oxide, rGO reduced graphene oxide, SEM scanning electron microscope, TEM transmission electron microscope

REFERENCES

(1) Zhang, Y.; Guo, L.; Wei, S.; He, Y.; Xia, H.; Chen, Q.; Sun, H.-B.; Xiao, F.-S. Direct Imprinting of Microcircuits on Graphene Oxides Film by Femtosecond Laser Reduction. *Nano Today* **2010**, *5*, 15–20.

(2) Sokolov, D. A.; Rouleau, C. M.; Geohegan, D. B.; Orlando, T. M. Excimer Laser Reduction and Patterning of Graphite Oxide. *Carbon* **2013**, *53*, 81–89.

(3) Kymakis, E.; Petridis, C.; Anthopoulos, T. D.; Stratakis, E. Laser-Assisted Reduction of Graphene Oxide for Flexible, Large-Area Optoelectronics. *IEEE Journal of Selected Topics in Quantum Electronics* **2014**, *20*, 106–115.

(4) Guan, Y.; Fang, Y.; Lim, G.; Zheng, H.; Hong, M. Fabrication of Laser-Reduced Graphene Oxide in Liquid Nitrogen Environment. *Scientific Reports* **2016**, *6*.

(5) Teoh, H. F.; Tao, Y.; Tok, E. S.; Ho, G. W.; Sow, C. H. Direct Laser-Enabled Graphene Oxide-Reduced Graphene Oxide Layered Structures with Micropatterning. *Journal of Applied Physics* **2012**, *112*, 064309.

(6) Petridis, C.; Lin, Y.-H.; Savva, K.; Eda, G.; Kymakis, E.; Anthopoulos, T.; Stratakis, E. Post-Fabrication, in Situ Laser Reduction of Graphene Oxide Devices. *Applied Physics Letters* **2013**, *102*, 093115.

(7) El-Kady, M. F.; Strong, V.; Dubin, S.; Kaner, R. B. Laser Scribing of High-Performance and Flexible Graphene-Based Electrochemical Capacitors. *Science* **2012**, *335*, 1326–1330.

(8) Strong, V.; Dubin, S.; El-Kady, M. F.; Lech, A.; Wang, Y.; Weiller, B. H.; Kaner, R. B. Patterning and Electronic Tuning of Laser Scribed Graphene for Flexible All-Carbon Devices. *ACS Nano* **2012**, *6*, 1395–1403.

(9) Inagaki, M.; Qiu, J.; Guo, Q. Carbon Foam: Preparation and Application. *Carbon* **2015**, *87*, 128–152.

(10) Henley, S.; Carey, J.; Silva, S.; Fuge, G.; Ashfold, M.; Anglos, D. Dynamics of Confined Plumes during Short and Ultrashort Pulsed Laser Ablation of Graphite. *Physical Review B* **2005**, *72*, 205413.

(11) Rode, A. V.; Hyde, S.; Gamaly, E.; Elliman, R.; McKenzie, D.; Bulcock, S. Structural Analysis of a Carbon Foam Formed by High Pulse-Rate Laser Ablation. *Applied Physics A: Materials Science & Processing* **1999**, *69*, S755–S758.

(12) Rode, A. V.; Gamaly, E. G.; Luther-Davies, B. Formation of Cluster-Assembled Carbon Nano-Foam by High-Repetition-Rate Laser Ablation. *Applied Physics A: Materials Science & Processing* **2000**, *70*, 135–144.

(13) Muñoz, E.; de Val, M.; Ruiz-González, M. L.; López-Gascón, C.; Sanjuán, M. L.; Martinez, M. T.; González-Calbet, J. M.; Germán, F.; Laguna, M. Gold/carbon Nanocomposite Foam. *Chemical physics letters* **2006**, *420*, 86–89.

(14) Zani, A.; Dellasega, D.; Russo, V.; Passoni, M. Ultra-Low Density Carbon Foams Produced by Pulsed Laser Deposition. *Carbon* **2013**, *56*, 358–365.

(15) Spanakis, E.; Pervolaraki, M.; Giapintzakis, J.; Katsarakis, N.; Koudoumas, E.; Vernardou, D. Effect of Gold and Silver Nanoislands on the Electrochemical Properties of Carbon Nanofoam. *Electrochimica Acta* **2013**, *111*, 305–313.

(16) Cao, C.; Hu, C.; Fang, L.; Wang, S.; Tian, Y.; Pan, C. Humidity Sensor Based on Multi-Walled Carbon Nanotube Thin Films. *Journal of Nanomaterials* **2011**, *2011*, 5.

(17) Chu, J.; Peng, X.; Feng, P.; Sheng, Y.; Zhang, J. Study of Humidity Sensors Based on Nanostructured Carbon Films Produced by Physical Vapor Deposition. *Sensors and Actuators B: Chemical* **2013**, *178*, 508–513.

(18) Wu, J.; Feng, S.; Wei, X.; Shen, J.; Lu, W.; Shi, H.; Tao, K.; Lu, S.; Sun, T.; Yu, L.; *et al.* Facile Synthesis of 3D Graphene Flowers for Ultrasensitive and Highly Reversible Gas Sensing. *Advanced Functional Materials* **2016**, *26*, 7462–7469.

(19) Asai, M.; Ohba, T.; Iwanaga, T.; Kanoh, H.; Endo, M.; Campos-Delgado, J.; Terrones, M.; Nakai, K.; Kaneko, K. Marked Adsorption Irreversibility of Graphitic Nanoribbons for CO2 and H2O. *Journal of the American Chemical Society* **2011**, *133*, 14880–14883.

(20) Lipatov, A.; Varezhnikov, A.; Wilson, P.; Sysoev, V.; Kolmakov, A.; Sinitskii, A. Highly Selective Gas Sensor Arrays Based on Thermally Reduced Graphene Oxide. *Nanoscale* **2013**, *5*, 5426–5434.

(21) Varghese, S. S.; Lonkar, S.; Singh, K.; Swaminathan, S.; Abdala, A. Recent Advances in Graphene Based Gas Sensors. *Sensors and Actuators B: Chemical* **2015**, *218*, 160–183.

(22) Cho, B.; Yoon, J.; Hahm, M. G.; Kim, D.-H.; Kim, A. R.; Kahng, Y. H.; Park, S.-W.; Lee, Y.-J.; Park, S.-G.; Kwon, J.-D.; *et al.* Graphene-Based Gas Sensor: Metal Decoration Effect and Application to a Flexible Device. *Journal of Materials Chemistry C* **2014**, *2*, 5280–5285.

(23) Ashfold, M. N.; Claeyssens, F.; Fuge, G. M.; Henley, S. J. Pulsed Laser Ablation and Deposition of Thin Films. *Chemical Society Reviews* **2004**, *33*, 23–31.

(24) Trusovas, R.; Ratautas, K.; Ravciukaitis, G.; Barkauskas, J.; Stankevivciene, I.; Niaura, G.; Mavzeikiene, R. Reduction of Graphite Oxide to Graphene with Laser Irradiation. *Carbon* **2013**, *52*, 574–582.

(25) Qian, M.; Zhou, Y. S.; Gao, Y.; Park, J. B.; Feng, T.; Huang, S. M.; Sun, Z.; Jiang, L.; Lu, Y. F. Formation of Graphene Sheets through Laser Exfoliation of Highly Ordered Pyrolytic Graphite. *Applied Physics Letters* **2011**, *98*, 173108.

(26) Ferrari, A. C.; Robertson, J. Interpretation of Raman Spectra of Disordered and Amorphous Carbon. *Physical review B* **2000**, *61*, 14095.

(27) Siegel, J.; Lyutakov, O.; Rybka, V.; Kolská, Z.; Svorčík, V. Properties of Gold Nanostructures Sputtered on Glass. *Nanoscale Res Lett* **2011**, *6*, 96.

(28) Lin, W.-D.; Chang, H.-M.; Wu, R.-J. Applied Novel Sensing Material Graphene/polypyrrole for Humidity Sensor. *Sensors and Actuators B: Chemical* **2013**, *181*, 326–331.

(29) Xue, Y. Water Monomer Interaction with Gold Nanoclusters from van Der Waals Density Functional Theory. *J Chem Phys* **2012**, *136*, 024702.

(30) Smith, A. D.; Elgammal, K.; Niklaus, F.; Delin, A.; Fischer, A. C.; Vaziri, S.; Forsberg, F.; Råsander, M.; Hugosson, H.; Bergqvist, L.; *et al.* Resistive Graphene Humidity Sensors with Rapid and Direct Electrical Readout. *Nanoscale* **2015**, *7*, 19099–19109.

(31) Hummers Jr, W. S.; Offeman, R. E. Preparation of Graphitic Oxide. *Journal of the American Chemical Society* **1958**, *80*, 1339–1339.

(32) Vallés, C.; Núñez, J. D.; Benito, A. M.; Maser, W. K. Flexible Conductive Graphene Paper Obtained by Direct and Gentle Annealing of Graphene Oxide Paper. *Carbon* **2012**,

50, 835–844.

TOC – FIGURE